Journal of
Synchrotron Radiation

ISSN 0909-0495

Received 22 February 2012
Accepted 11 June 2012

Valence structures of aromatic bioactive compounds: a combined theoretical and experimental study

Anoja Pushpamali Wickrama Arachchilage,[a] Vitaliy Feyer,[b] Oksana Plekan,[b]‡ Marianna Iakhnenko,[b,c] Kevin C. Prince[b,d] and Feng Wang[a]*

[a]eChemistry Laboratory, Faculty of Life and Social Sciences, Swinburne University of Technology, Howthron, Melbourne, Victoria 3122, Australia, [b]Sincrotrone Trieste, Area Science Park, I-34012 Basovizza, Trieste, Italy, [c]Taras Shevchenko National University of Kyiv, Faculty of Physics, Department of Experimental Physics, Academician Glushkov Avenue 4, Kyiv, Ukraine, and [d]Istituto Officina dei Materiali, Consiglio Nazionale delle Ricerche, Area Science Park, I-34149 Trieste, Italy. E-mail: fwang@swin.edu.au

Valence electronic structures of three recently isolated aryl bioactive compounds, namely 2-phenylethanol (2PE), *p*-hydroxyphenylethanol (HPE) and 4-hydroxybenzaldehyde (HBA), are studied using a combined theoretical and experimental method. Density functional theory-based calculations indicate that the side chains cause electron charge redistribution and therefore influence the aromaticity of the benzene derivatives. The simulated IR spectra further reveal features induced by the side chains. Solvent effects on the IR spectra are simulated using the polarizable continuum model, which exhibits enhancement of the O—H stretch vibrations with significant red-shift of 464 cm^{-1} in 2PE. A significant spectral peak splitting of 94 cm^{-1} between O(4)—H and O(8)—H of HPE is revealed in an aqueous environment. Experimental measurements for valence binding energy spectra for 2PE, HPE and HBA are presented and analyzed using outer-valence Green function calculations. The experimental (predicted) first ionization energies are measured as 9.19 (8.79), 8.47 (8.27) and 8.97 (8.82) eV for 2PE, HPE and HBA, respectively. The frontier orbitals (highest occupied molecular orbitals, HOMOs, and lowest unoccupied molecular orbitals, LUMOs) have similar atomic orbital characters although the HOMO–LUMO energy gaps are quite different.

Keywords: electronic structures; binding energy spectra; bioactive compounds; spectroscopic studies; theory and experiment.

1. Introduction

Natural products are a rich source of many active ingredients in medicines and new drugs (Chen *et al.*, 2010). Some compounds recently isolated from several marine fungi, such as *Arthrinium saccharicola*, *Cladosporium sp.* and *Ampelomyces sp.*, namely benzene derivatives such as 2-phenylethanol (2PE), *p*-hydroxyphenylethanol (HPE, also known as *p*-tyrosol) and 4-hydroxybenzaldehyde (HBA), have shown antifouling activities (Li, 2006). While 2PE and HPE possess a hydroxyethyl side chain ($–CH_2CH_2OH$) attached to either a phenyl or a phenol fragment, HBA has an aldehyde group (–CH═O) attached to the *para*-position of the phenol ring, representing a common structural motif in many bioactive compounds (Robertson & Simons, 2000; Bowman, 2007).

As an aroma compound (Fronza *et al.*, 2009) of many natural products, 2PE is also a major constituent found in rose-like or honey flavor (Sakai *et al.*, 2007; Tieman *et al.*, 2007) and in other contexts such as insect pheromones (Jirovetz *et al.*, 2008). 2PE also exhibits antibacterial activity (Jacobson *et al.*, 2005; Berrah & Konetzka, 1962) and induces inhibition of viral DNA synthesis (Müller *et al.*, 2005). As a hydroxy analogue of the neurotransmitter 2-phenylethylamine (Karaminkov *et al.*, 2008; Panja & Chakraborty, 2003), 2PE is also considered as a prototype molecule for neurotransmitters. Some experimental data are available for 2PE, such as gas-phase IR spectra (Fang & Swofford, 1984), as well as UV hole burning studies (Mons *et al.*, 1999). Moreover, the hydrated complexes of 2PE and its intramolecular and intermolecular hydrogen bond networks have been studied (Karaminkov *et al.*, 2008; Mons *et al.*, 1999; Bakke & Chadwick, 1988; Chervenkov *et al.*, 2006; Mardis *et al.*, 2000).

‡ Present address: Aarhus University, Department of Physics and Astronomy, Ny Munkegade 120, 8000 Aarhus C, Denmark.

HPE exerts mild antioxidant effects in natural products such as wine and virgin olive oil (Hockridge *et al.*, 1998; Cui *et al.*, 2003; Guzman-Lopez *et al.*, 2007). It has been used in the treatment of atherosclerosis, protecting low-density lipoproteins from oxidation (Liu & Mori, 1993). The antioxidant ability of HPE is corroborated by its radical scavenging ability against DPPH (1,1-diphenyl-2-picryl hydrazyl) radicals, superoxide and hydroxyl radicals (Ahn *et al.*, 2008). A recent experiment (Wiseman *et al.*, 2002) confirmed the cytotoxity of HPE against human cancer cells and suggested its applications as a potential anticancer drug candidate. From a chemical structure point of view, HPE differs from 2PE only by a hydroxyl (OH) moiety attached at the *para*-position of the phenyl ring. However, their chemical properties and pharmaceutical functions are quite different, with HPE being less studied than 2PE. As an analogue of HPE and 2PE, HBA functions as an anticonvulsant owing to its inhibitory effect against GABA transaminase (Ha *et al.*, 2000). It is able to prevent ischemic neuronal cell death in the hippocampal CA1 region of the brain (Kim *et al.*, 2007). The crystal structure (Iwasaki, 1977; Jasinski *et al.*, 2008) and IR spectra (Ehrhardt, 1984) of HBA have been reported.

Gas-phase studies play an important role in elucidating structures and dynamics of biomolecules (Wang *et al.*, 2008), while solvent effect studies provide insight into chemical equilibrium and the rate of chemical reactions (Dharmalingam *et al.*, 2006). This study will describe environmental effects on these bioactive compounds through simulated IR spectra in various solvents including polar and non-polar solvents. In order to understand the effects of side chains on the chemical properties of the molecules, it is important to reveal their electronic properties and interactions of the side chains with the aromatic ring of the molecules. This is done using soft photoemission spectroscopy (PES) combined with quantum mechanical calculations.

2. Experimental methods and computational details

The valence ionization spectral measurements of HBA, HPE and 2PE were performed at the gas-phase photoemission beamline, Elettra, Trieste (Italy), using apparatus and calibration methods described previously (Plekan *et al.*, 2007*a*,*b*,*c*). The beamline is equipped with a six-channel 150 mm hemispherical electron energy analyser, mounted in the plane defined by the (linearly polarized) electric vector of the light and the photon propagation direction at an angle of 54.7° with respect to the electric vector of the light (the so-called pseudo magic angle). In this geometry the measurements should be insensitive to the photoelectron asymmetry parameter β. The spectra were measured with a total resolution (photons + analyzer) of 0.45 eV at $h\nu$ = 99 eV.

The compounds were supplied by Sigma-Aldrich and used without further purification. HBA, 2PE and HPE were evaporated at 325 K, 295 K (ambient temperature) and 319 K, respectively. At these low temperatures thermal decomposition is not expected, but the samples were checked for spectral changes as a function of time and discoloration after heating *etc*. No evidence was found for decomposition of the compounds. Traces of water contamination which decreased slowly with time but did not vanish entirely were present in the HPE sample. The HPE spectra were obtained by subtraction of the spectrum of water from the raw data.

All geometry optimizations were performed using the density functional theory (DFT)-based B3LYP/cc-pVTZ model, which is incorporated in the *GAMESS* computational chemistry package (Schmidt *et al.*, 1993), followed by harmonic vibrational frequency calculations using the *Gaussian03* computational package (Frisch *et al.*, 2004). The optimized geometries of the species are true minimum configurations without any imaginary frequencies. IR spectra were produced based on the optimized geometries using the same model. Solvent effects on the IR spectra of 2PE, HPE and HBA were calculated in polar and non-polar solvents, *i.e.* water (H_2O, ε = 78.36) and carbon tetrachloride (CCl_4, ε = 2.23), respectively, using the polarizable continuum model (Cossi *et al.*, 1996). Other properties such as molecular electrostatic potentials and Hirshfeld charges (Hirshfeld, 1977; Ayers, 2006) were calculated using the B3LYP/cc-pVTZ and LB94/et-pVQZ models (Chong *et al.*, 2004; van Leeuwen & Baerends, 1994), respectively. Valence vertical ionization energies of the species were then carried out using the outer-valence Green function (OVGF) (Cederbaum, 1975; Cederbaum & Domcke, 1977; von Niessen *et al.*, 1984; Zakrzewski & von Niessen, 1993; Zakrzewski & Ortiz, 1995), incorporating the cc-pVTZ basis set, *i.e.* the OVGF/cc-pVTZ//B3LYP/cc-pVTZ model and the Hartree–Fock (HF)/cc-pVTZ model in the *Gaussian03* computational package.

3. Results and discussion

3.1. Geometric properties and charge distributions

The optimized structures of three benzene derivatives, 2-phenylethanol (2PE), *p*-hydroxyphenylethanol (HPE) and 4-hydroxybenzaldehyde (HBA), are presented in Fig. 1, together with the Hirshfeld charges for non-H atoms (in parentheses). 2PE and HPE are phenylethanol analogues that

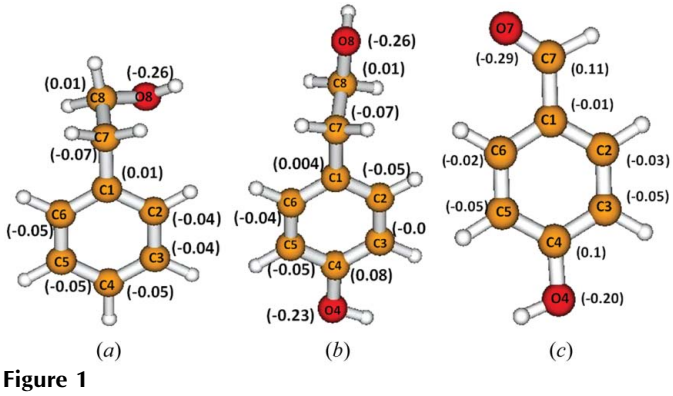

Figure 1
Two-dimensional view of optimized structures of (*a*) 2-phenylethanol (2PE), (*b*) *p*-hydroxyphenylethanol (HPE) and (*c*) 4-hydroxybenzaldehyde (HBA) with atomic numbering. The Hirshfeld charges are indicated in parentheses.

Table 1
Calculated geometric properties of 2-phenylethanol (2PE), *p*-hydroxyphenylethanol (HPE) and 4-hydroxybenzaldehyde (HBA), and experimental values for HBA.

	2PE			HPE	HBA	
	This work†	PW91‡	MNDO§	This work†	This work†	Exp¶
C(1)—C(7) (Å)	1.51			1.51	1.46	
C(4)—O(4) (Å)				1.37	1.34	
R_6 (Å)	8.35			8.35	8.34	8.34
∠C(6)C(1)C(2) (°)	118.25			117.38	118.70	118.39
∠O(8)C(8)C(7) (°)	113.79			108.05		
∠C(7)C(1)C(2) (°)	121.33			120.61	120.25	118.97
∠C(8)C(7)C(1)C(2) (λ1) (°)	89.84	95.2	95.9	76.25		
∠O(8)C(8)C(7)C(1) (λ2) (°)	−64.19	61.0	−65.7	−176.46		
∠H(8)O(8)C(8)C(7) (λ3) (°)	292.8	297.8	79.6	182.24		
∠C(2)C(3)C(4)C(5) (°)	−0.08			−0.19	0.00	0.31
∠H(4)O(4)C(4)C(5) (°)				−179.32	0.00	
μ (D)	1.62			2.03	3.45	

† The B3LYP/cc-pVTZ model. ‡ Patey & Dessent (2002). § Bakke & Chadwick (1988). ¶ Jasinski *et al.* (2008).

differ by a hydroxyl group attached to the *para*-position of the HPE aromatic ring. On the other hand, HPE and HBA are phenol analogues including hydroxyethyl and aldehyde groups, respectively, at the C(1) site. Hence, the three compounds share certain geometric and chemical characteristics.

The optimized geometrical parameters and other properties such as dipole moments of 2PE, HPE and HBA are listed and compared in Table 1. Much attention has been paid to the stable conformations (*gauche* and *anti*) of 2PE with respect to the side chain $-CH_2CH_2OH$ (Robertson & Simons, 2000; Karaminkov *et al.*, 2008; Mons *et al.*, 1999, 2000; Bakke & Chadwick, 1988; Dickinson *et al.*, 1998; Patey & Dessent, 2002; Guchhait *et al.*, 1999). Properties of the more stable *gauche* conformer (Godfrey *et al.*, 1999) will be studied in this work. The total energy of 2PE is −385.996213 E_h (Hartrees), using the B3LYP/cc-pVTZ model, which is 1.18 eV lower than a previous theoretical calculation based on the PW91/cc-pVDZ model (Patey & Dessent, 2002) and 29.47 eV lower than the value using the MP2/cc-pVDZ model (Patey & Dessent, 2002). The dihedral angles, λ_1 [C(8)C(7)C(1)C(2)], λ_2 [O(8)C(8)C(7)C(1)] and λ_3 [H(8)O(8)C(8)C(7)], which describe the orientation of the hydroxyethyl side chain of 2PE (refer to Table 1), agree well with previous calculations using either semi-empirical (MNDO) (Bakke & Chadwick, 1988) or DFT-based PW91 (Patey & Dessent, 2002) methods (see Table 1).

In contrast to the *gauche* orientation of 2PE, we find the *anti* conformation of HPE is more stable, which is in agreement with a previous study (Hockridge *et al.*, 1998). While other angles exhibit small alterations, the dihedral angles λ_2 and λ_3, which are primarily responsible for the *gauche* and the *anti* orientation, are quite different in HPE, compared with 2PE. The stable conformer of HBA exhibits a planar structure according to the present study, which is in agreement with a recent study (Sajan *et al.*, 2010) based on the B3LYP/6–311++G(d,p) model. In Table 1 the calculated ring perimeter (R_6) (Wang *et al.*, 2005) and bond angles of HBA exhibit good agreement with the crystal structure (Dickinson *et al.*, 1997), and simulated dihedral angles of this study exhibit the planar shape of the molecule, which also agrees with the previous calculation (Sajan *et al.*, 2010).

The simulated aromatic ring perimeters (Wang *et al.*, 2005), R_6, remain unchanged with respect to benzene at 8.35 Å in 2PE and HPE (Wickrama Arachchilage *et al.*, 2011), using the same model. This indicates that the bond with hydroxyethyl and/or hydroxyl side chain(s) in 2PE and HPE does not directly affect the bond lengths of the phenyl ring significantly. Different side chains, such as hydroxyethyl and aldehyde, bonding at the C(1) site of the molecules alters the distance of C(1)—C(7), but the impact of the *para* hydroxyl group is insignificant. For example, the bond lengths C(1)—C(7) of 2PE and HPE, in which a hydroxyethyl chain bonds at the C(1) site, remains the same (1.51 Å), while the distance is reduced in HBA (1.46 Å) owing to the influence of the aldehyde group (CH═O) at the same site. Evidently, the C═O fragment of HBA contracts the aromatic-ring and side-chain bond lengths of the molecule by a small amount. The side-chain bonding of these benzene derivatives affects all bond angles of the aromatic ring, so that they diverge slightly from the free benzene bond angles of 120°. For example, the bond angle ∠C(6)C(1)C(2) of 2PE, HPE and HBA is distorted from the value of benzene to 118.25°, 117.38° and 118.70°, respectively. Apparently, the plane formed by C(8), C(7) and C(1) is almost perpendicular to the phenyl plane in HPE, which is not the case in 2PE, indicating the phenol impact on the geometry of HPE.

The most significant effect of the side chains on the aromatic compounds is their dipole moment. Side chains such as aldehyde, hydroxyethyl and hydroxyl groups reduce the high symmetry of the unsubstituted benzene and confer a dipole moment on the derivatives. For example, the dipole moments of 2PE, HPE and HBA are 1.62 D, 2.03 D and 3.45 D, respectively. This is due to the OH group in the *para* position of the aromatic ring of HPE, causing an increase of approximately 0.4 D with respect to 2PE. The aldehyde (–CH═O) in HBA directly connected with the phenyl ring results in the largest dipole moment of 3.45 D among the compounds in this study.

Atomic site-specific Hirshfeld charges (Q^H) of the non-H atoms are given in Fig. 1. In the benzene ring the C atoms possess negative charges when bonded with H atoms, whereas the charges of C atoms in the C—O bonds are positive. For example, the C(4) sites in HPE and HBA are positively charged by 0.08 a.u. and 0.10 a.u., compared with −0.05 a.u. in 2PE. The difference in electronegativity between C and O of the side chain leads to both σ and π electron transfer from C to O, so that the C atoms directly connected to O become positively charged. Substituents with lone pairs may also transfer π electron density to the electron-deficient phenyl ring (Wiberg

et al., 1999), causing charge redistribution, which is reflected by the Hirshfeld charges of the phenyl C atoms. The effect of the aldehyde group on the charge distribution of the phenyl ring in HBA is distinctive. The C atoms in the half of the phenyl ring closest to the aldehyde, C(6), C(1) and C(2), are more negatively charged in HBA, compared with 2PE and HPE. The Q^{H} values on O(8), C(8) and C(7) are exactly the same in 2PE and HPE. We attribute this to charge transfer by hybridization of the aldehyde and phenyl π systems. Evidently the charge delocalization is not complete, and occurs mainly in one half of the phenyl ring. The charge redistribution of the derivatives with respect to unsubstituted benzene (Wickrama Arachchilage *et al.*, 2011) suggests redistribution of the charge density owing to the distortion of π-conjugation (Cyrański, 2005).

Fig. 2 shows two-dimensional molecular electrostatic potentials (MEPs) of 2PE, HPE and HBA in both the phenyl plane and the plane formed by the side chain H(8)–O(8)–C(8)–C(7). The latter plane provides a side view for the non-planar molecules (note that HBA is planar so that a side view is not necessary). In the phenyl plane of the MEPs, similarities and differences between the molecules are apparent. For example, MEPs of 2PE (Fig. 2*a*) form closed loops in the phenyl plane and the side chain. In HPE and HBA the most obvious differences are that the additional hydroxyl group at the *para*-position, C(4), of the phenyl ring opens the MEP loops at the O(4) and O(8) oxygen sites [as shown by the side view of HPE in Figs. 2(*b*) and 2(*c*)]. As a result it is possible that HPE and HBA with strongly negative MEP regions are able to form stronger hydrogen bonds or can be subjected to electrophilic attack as these oxygen sites of the molecules can attract protons.

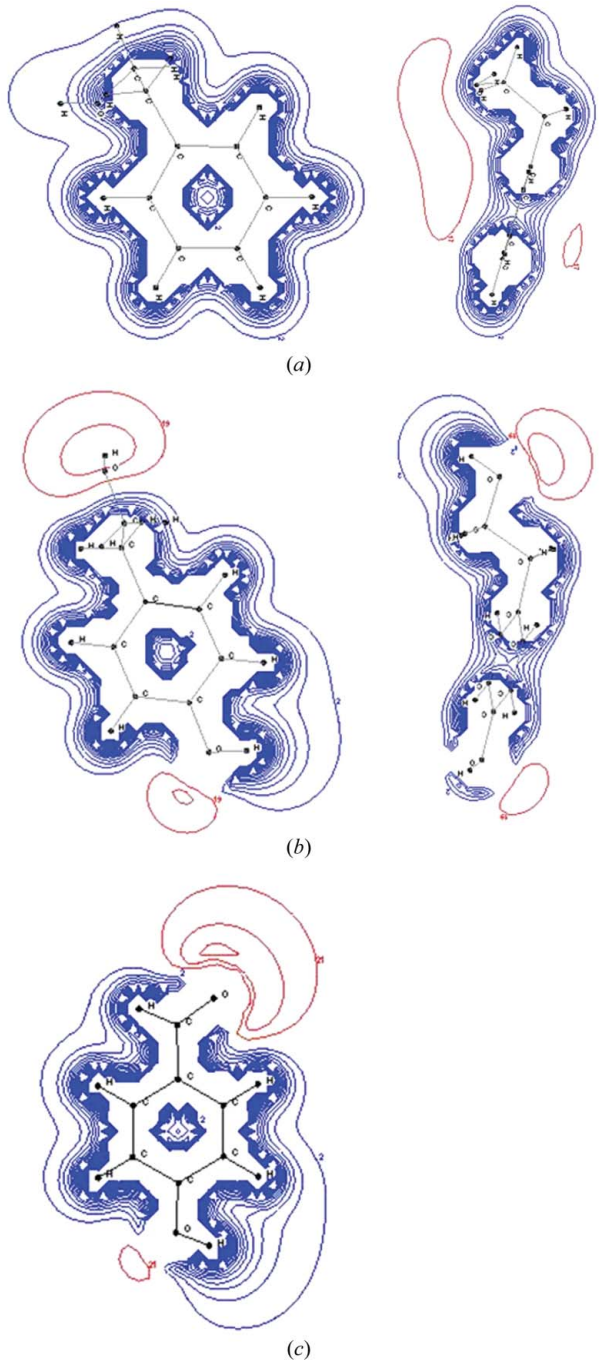

Figure 2
Molecular electrostatic potential (MEP) of (*a*) 2PE, (*b*) HPE and (*c*) HBA.

3.2. Vibrational spectroscopy

Fig. 3(*a*) compares the simulated IR spectra of 2PE, HPE and HBA with the available experimental IR spectra of 2PE and HBA (NIST, 2009) in the gas phase. A scaling factor for the wavenumber axis of 0.96 (Scott & Radom, 1996; Huang *et al.*, 2006) has been applied based on the O—H stretch frequency. Good agreement between the simulated and experimental IR spectra of 2PE and HBA is observed, which indicates that the present model (B3LYP/cc-pVTZ) is sufficiently accurate after scaling. Experimental and/or theoretical gas-phase IR spectra of 2PE (Fang & Swofford, 1984; Mons *et al.*, 1999; Guchhait *et al.*, 1999) and HBA (Ehrhardt, 1984; Mart *et al.*, 2004) are available, but no detailed IR spectra are available for HPE to our knowledge, although some far-IR (low-frequency) vibrational features (Hockridge *et al.*, 1998) and a condensed-phase FT-IR spectrum (Pouchert, 1985) exist. An assignment of the major IR spectral peaks, together with the available measurements, is given in Table 2.

The patterns of the simulated IR spectra in Fig. 3(*a*) show similarities, because the three biomolecules are related. For example, the region above 2700 cm^{-1} is dominated by C—H (2800–3100 cm^{-1}) and O—H (3600–3700 cm^{-1}) stretch modes because the three species contain the same functional groups in different chemical environments. For example, a single hydroxyl group in the molecular structures of 2PE and HBA contributes to the O—H stretch peak at 3662 cm^{-1} and 3654 cm^{-1}, respectively, in each spectrum, whereas in HPE two hydroxyl groups contribute to the O—H stretch peak at 3671/3680 cm^{-1}. The C—H stretch region at 2800–3100 cm^{-1} exhibits side-chain specific dissimilarities. For example, a broad spectral peak in 2PE and HPE represents the C—H stretch frequencies of side-chain and aromatic C atoms. However, a single peak in HBA at 2753 cm^{-1} corresponds to

Table 2
IR assignment of 2-phenylethanol (2PE), *p*-hydroxyphenylethanol (HPE) and 4-hydroxybenzaldehyde (HBA) (cm^{-1}).

	2PE		HPE	HBA	
Mode	This work†	Exp‡	This work†	This work†	Exp‡
O(8)—H stretch	3662	3670/3626§/3660¶	3680		
O(4)—H stretch			3671	3654	3650
Ring C—H stretch	3061–3025	3110–2990	3060–3015	3072–3029	
Side-chain C—H stretch	2952–2862	2990–2870	2956–2858	2753	
C(7)═O(7) stretch				1698	1730
C—C and/or C═C stretch	1580–1560		1592–1490	1581	1610
C(4)—O(4) stretch			1234	1517	
C(8)—O(8) stretch	1033	1030	1012		
O(8)—H bend	974		1187		
O(4)—H bend			1143	1149	1170
Ring CH—CH scissoring				1134	
Ring C—H bend	689	710	830, 817	820	850

† The B3LYP/cc-pVTZ model. ‡ NIST (2009). § Mons *et al.* (1999). ¶ Fang & Swofford (1984).

the side-chain C(7)—H stretch frequency. The carbonyl C(7)═O group of HBA directly affects the C(7)—H stretch frequency by a red-shift of 105 cm^{-1} from the ring C—H frequencies.

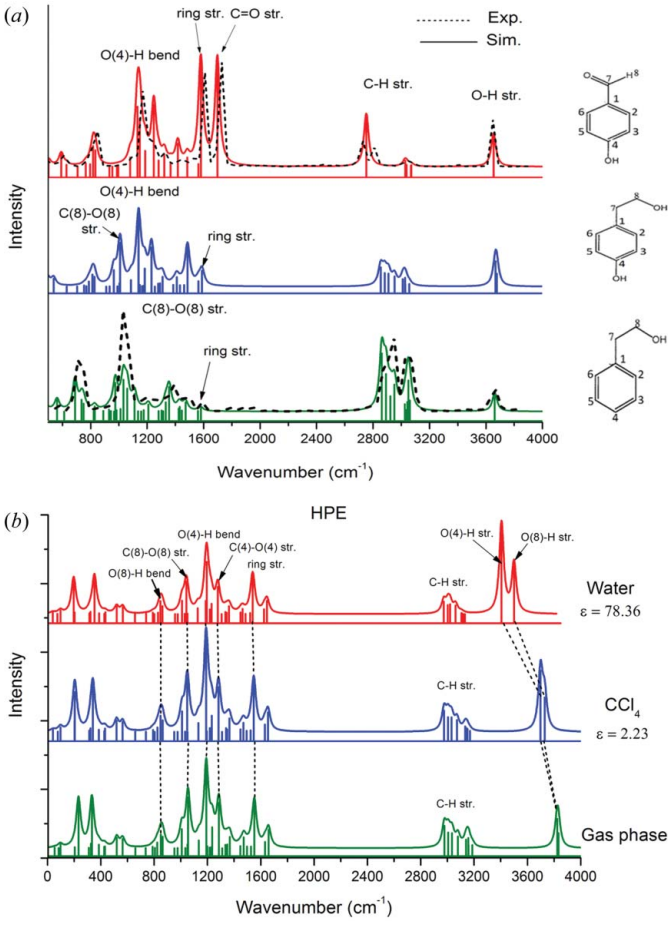

Figure 3
(*a*) Comparative experimental gas-phase [dashed lines from NIST Chemistry WebBook (http://webbook.nist.gov/)] and simulated gas-phase (full line) IR spectra of 2PE (lower), HPE (middle) and HBA (upper). A scaling factor of 0.96 has been applied based on the OH stretch frequency. (*b*) Solvent effect on HPE IR spectra.

The frequency region 500–1700 cm^{-1} in the IR spectra of the compounds is identified as their fingerprint region, and exhibits site-specific differences as the major IR peaks are due to the vibrations caused by the side chains. For example, the long side chains and the aromatic ring of 2PE and HPE are composed of a number of C—C/C═C, C—H and C—O bonds, which exhibit combination vibrational frequencies in this region. The *para*-OH group in HPE significantly enhances the C(4)—O stretch mode of HPE and HBA. In addition to the ring stretch vibrations at 1600 cm^{-1} of HBA, similar to 2PE and HPE, a dominant peak at 1700 cm^{-1} is observed only in the HBA spectrum corresponding to the C═O stretch frequency, which is characteristic of benzaldehyde derivatives.

Solvents play an important role in the IR spectra of biomolecules (Wickrama Arachchilage *et al.*, 2011; Selvam *et al.*, 2010; Jalkanen *et al.*, 2008). As a result, solvent effects on the IR spectra of the compounds were studied using the polarizable continuum model (PCM). A polar solvent (water, ε = 78.36) and non-polar solvent [tetrachloromethane (CCl_4), ε = 2.23] were employed in this PCM model. Fig. 3(*b*) compares the solvent effects on IR spectra of HPE with respect to the gas phase. The simulated IR spectra of 2PE and HBA in solvents and the gas phase are given in the supplementary material (Figs. S1 and S2).[1] The most significant changes in the IR spectra in Fig. 3(*b*) due to solvents are the apparent red-shift and splitting of the O–H stretch spectral peaks.

Other IR spectral peaks of HPE under 3200 cm^{-1} and their patterns are minimally affected by the solvents. The red-shifts ($\Delta\upsilon$) owing to solvents in the O–H stretch vibrations are more apparent in water (polar solvent) than in CCl_4 (non-polar solvent) with respect to the gas phase, which is also observed in the IR spectra of 3-chloro-2,5-dihydroxybenzyl alcohol (Wickrama Arachchilage *et al.*, 2011). For example, $\Delta\upsilon$[O(8)–H] is red-shifted by 104 and 333 cm^{-1} in CCl_4 and water, respectively, with respect to the gas phase, which may be due to intermolecular hydrogen bonding between the lone pair of oxygen and the hydrogen of water molecules (Mons *et al.*, 1999). Moreover, the two O–H stretch vibrations of HPE, *i.e.* υ[O(4)–H] and υ[O(8)–H], split significantly in solvents. For example, the splitting $\delta\upsilon$ between υ[O(4)–H] and υ[O(8)–H] is 9 cm^{-1} in the gas phase, but it becomes 30 cm^{-1} in CCl_4 and 94 cm^{-1} in water. Such significant splitting indicates different intermolecular interactions of the hydroxyl groups in HPE with the solvent molecules. The solvent effects also contribute to the enhancement of the IR intensities of the O–H stretch

[1] Supplementary data for this paper are available from the IUCr electronic archives (Reference: VV5041). Services for accessing these data are described at the back of the journal.

Table 3
The assignment of vertical ionization energies in valence space of 2PE, HPE and HBA (eV).

2PE				HPE				HBA			
Orbital	HF†	OVGF†‡	Exp	Orbital	HF†	OVGF†‡	Exp	Orbital	HF†	OVGF†‡	Exp
33*a*§	8.80	8.79 (0.89)	9.19	37*a*§	8.36	8.27 (0.89)	8.47	5*a*″§	9.01	8.84 (0.89)	8.97
32*a*	9.04	9.05 (0.89)		36*a*	9.34	9.22 (0.89)	9.41	4*a*″	9.92	9.73 (0.89)	9.67
31*a*	12.05	10.72 (0.90)	10.45	35*a*	12.07	10.87 (0.91)	10.42	27*a*′	11.53	10.01 (0.88)	
30*a*	12.90	11.75 (0.89)	11.95	34*a*	12.75	11.47 (0.86)	11.37	3*a*″	13.23	12.02 (0.84)	11.70
29*a*	13.14	11.82 (0.90)		33*a*	13.23	11.84 (0.90)		26*a*′	13.79	12.35 (0.90)	12.08
28*a*	13.53	12.11 (0.85)		32*a*	13.53	12.09 (0.89)	12.41	2*a*″	14.88	13.74 (0.84)	13.53
27*a*	13.67	12.46 (0.88)	12.63	31*a*	13.72	12.39 (0.89)		25*a*′	15.35	13.51 (0.89)	–
26*a*	14.23	13.10 (0.90)	–	30*a*	14.18	12.87 (0.90)		1*a*″	15.96	14.16 (0.89)	–
25*a*	15.32	13.75 (0.88)	–	29*a*	15.45	13.86 (0.89)	13.63	24*a*′	16.56	14.86 (0.85)	14.63
24*a*	15.81	14.24 (0.88)	14.6	28*a*	15.75	14.33 (0.89)	14.27	23*a*′	16.78	14.76 (0.88)	
23*a*	16.41	14.82 (0.89)		27*a*	16.00	14.38 (0.88)		22*a*′	17.06	15.20 (0.87)	–
22*a*	16.65	15.02 (0.88)	15.4	26*a*	16.09	14.31 (0.85)		21*a*′	17.40	15.49 (0.88)	15.95
21*a*	17.05	15.37 (0.87)		25*a*	16.42	14.71 (0.88)	15.01	20*a*′	18.19	16.01 (0.87)	–
20*a*	17.55	15.76 (0.88)		24*a*	17.28	15.53 (0.88)	15.60	19*a*′	19.43	17.18 (0.86)	17.79
19*a*	18.38	16.71 (0.88)	16.80	23*a*	17.41	15.76 (0.89)		18*a*′	20.61	18.53 (0.86)	18.55
18*a*	19.09	17.28 (0.86)	–	22*a*	18.36	16.40 (0.88)	–	17*a*′	21.64		–
17*a*	21.54		18.73	21*a*	19.09	17.50 (0.89)	17.28	16*a*′	23.64		20.16
16*a*	22.40			20*a*	19.96	18.04 (0.86)	17.49	15*a*′	24.30		–
15*a*	23.46		20.32	19*a*	21.64		18.65	14*a*′	28.34		23.09
14*a*	26.53		22.35	18*a*	23.01		19.46	13*a*′	28.42		–
13*a*	27.48			17*a*	23.26		19.46	12*a*′	31.92		26.47
12*a*	28.79		24.09	16*a*	26.38		20.54	11*a*′	37.55		–
11*a*	31.35		26.11	15*a*	27.75		22.50	10*a*′	39.11		32.89
10*a*	36.93		32.00	14*a*	28.73		24.10				
				13*a*	31.41		25.79				
				12*a*	36.88		32.11				
				11*a*	38.18						

† cc-pVTZ. ‡ The pole strength values are in parantheses. § HOMO.

vibrations, in relation to the dielectric constant of solvents. For example, the intensities of the υ(O–H) bands of HPE in water is almost double the values in the gas phase.

3.3. Photoionization spectroscopy

Although considerable data are available, assignments of spectral features benefit by comparison with theoretical calculations, which provide more detailed insight. This is particularly the case for soft photoionization spectra (PES), owing to the link between the electronic structure and the PES. Table 3 reports the vertical ionization energies of 2PE, HPE and HBA obtained from our experiment and theoretical calculations. The calculations are obtained using the OVGF/cc-pVTZ model for the outer valence space and the HF/cc-pVTZ model for the complete valence space for comparison. The OVGF model reproduces the ionization potential (IP) and agrees well with the measurement in the energy region of the IP up to 18 eV, whereas the inner-valence energy region can be estimated using the HF model. The inner-valence region contains emission from many excited states (two-hole, single-particle states) (Stenuit *et al.*, 2010), which the HF calculations do not predict, but they serve as a guide for identifying single-hole states. Owing to the small energy separations of the valence energy levels of the compounds, the measured PES spectra are considerably congested. For example, the first peak of 2PE at 9.19 eV in the measurement consists of two states of energies 8.79 eV (HOMO) and 9.05 eV (HOMO-1) based on our OVGF calculations (8.80 eV and 9.04 eV by the HF model). The spectroscopic pole strengths of HOMO and HOMO-1 are both 0.89, indicating that the single-particle picture is a good approximation in the model. This is also seen in the PES of L-phenylalanine (Ganesan *et al.*, 2011) and other benzene derivatives such as chlorobenzene and hydroquinone (Wickrama Arachchilage *et al.*, 2011).

The theoretical energies of the HOMOs match the experimental values quite well in all cases, and this is also true for HOMO-1 of 2PE. For HOMO-2 of 2PE, as well as the second- and third-highest orbitals of HPE and HBA, the theoretical values of the ionization energies are higher than the experimental values by about half an electronvolt. Considering the higher binding energy ionic states, this seems to be a general offset rather than an expansion of the energy scale. The calculations predict density of states rather than the cross sections so we do not expect agreement for the intensities, and only attempt to assign peaks by their energy.

Fig. 4 compares the measured and simulated ionization spectra of 2PE, HPE and HBA, and Fig. S3 of the supplementary information shows the spectra including the inner valence band and O 2*s* state. The simulation in Fig. 4 is based on the IPs calculated using the OVGF/cc-pVTZ model in Table 3, with Gaussian line shape and full width at half-maximum (FWHM) of 1.00 eV in order to mimic the measured spectra. As seen in the spectra, the theory reproduces the major features in the experimental ionization spectra of 2PE, HPE and HBA in the outer-valence region IP < 18 eV. The first broad peak of 2PE is due to ionization of

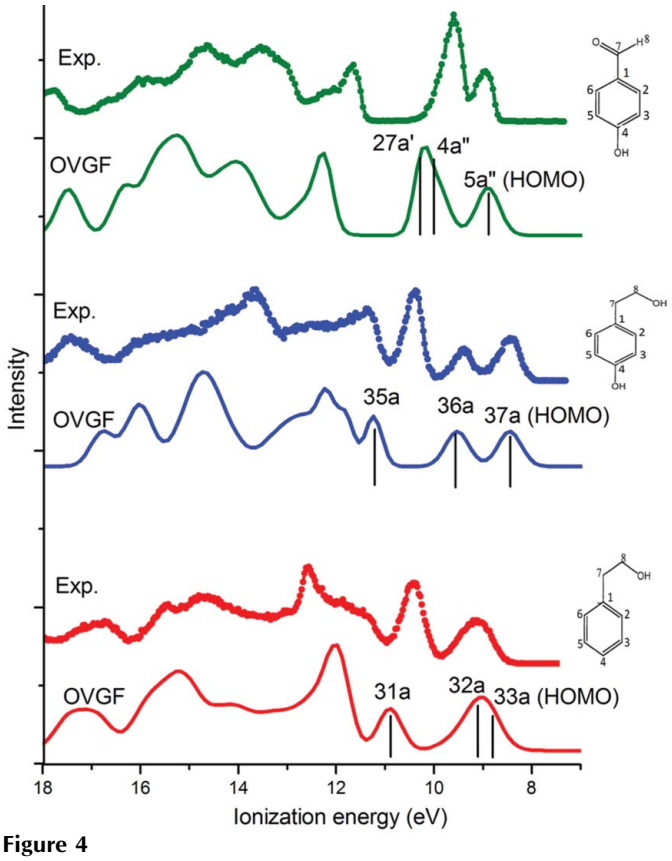

Figure 4
Experimental (dotted) and simulated (OVGF/cc-pVTZ) (thick line) valence ionization spectra of 2PE, HPE and HBA.

two orbitals, and the second peak is due to a single orbital. The current model of theory slightly underestimates the energy difference between the third- and fourth-highest molecular orbitals, and at higher energy there is a spectrally crowded region with many ionization states. The theory correctly predicts the dip at about 16 eV and shows that the broad peak at about 17 eV is due to two ionic states.

For HPE the first three peaks are due to ionization of the three highest lying molecular orbitals, after which there is again a congested region of many orbitals. The dip appearing at about 16.7 eV is correctly predicted. The first peak of HBA is due to ionization of the HOMO, but the second peak is once again due to two unresolved ionic states. The third peak and the broad feature next to it are due to single states. The present model of theory seems to overestimate the binding energies of the higher-energy part of the spectrum, with the result that, at the experimental minimum found around 17.2 eV, there is a peak. This presumably corresponds to a lower-energy feature. Since the central part of the measured valence spectra is not resolved because of rotational and vibrational broadening and spectral congestion, only the frontier orbital region IP < 11 eV will be analyzed in more detail.

The frontier orbital region consists of three outermost valence orbitals, namely the HOMO, the second HOMO (HOMO-1) and the third HOMO (HOMO-2). Fig. 5 shows an energy correlation diagram of the frontier orbitals of 2PE, HPE and HBA as well as their LUMO. As seen in this figure, although the HOMO–LUMO energy gaps and binding energies of the compounds vary, they all have the common characteristics that the LUMOs, HOMOs and HOMO-1 orbitals are dominated by the phenyl ring, whereas the HOMO-2 are dominated by the side chains of the derivatives. Other phenyl derivatives such as 3-chloro-2,5-dihydroxybenzyl alcohol and some of its derivatives (Wickrama Arachchilage *et al.*, 2011) show similar characteristics in their frontier orbitals. In fact, the HOMO and HOMO-1 for 2PE, HPE and HBA result from the splitting of the doubly degenerate HOMO of benzene. The C(4)—OH group at the *para*-position of the phenyl ring in HPE and HBA obviously contributes to large HOMO and HOMO-1 energy splitting: 0.95 eV for HPE and 0.89 eV for HBA, compared with 0.26 eV for 2PE without the OH group. The HOMO-2, 31*a* for 2PE, 35*a* for HPE and 27*a*′ for HBA, is dominated by the side chain of the compounds as shown by the orbitals in this figure. Their energies depend on the interactions between the oxygen on the side chain and the ring. The polarized carbonyl group in HBA weakens the interaction so that its HOMO-2 exhibits apparently smaller IPs than its counterpart in 2PE and HPE.

The plots of the charge density in Fig. 5 allow us to assign the character of the orbitals, and indicate that the HOMOs and HOMO-1s of all three compounds are composed of very similar benzene-derived π orbitals. The HOMO-2 orbital is dominated by ethanol (oxygen and carbon) lone-pair orbitals for 2PE and HPE. For HBA this orbital is also localized on the carbonyl oxygen; however, with a complex mixture of O 2*p*, C(7) 2*p* and C(1) 2*p* orbitals.

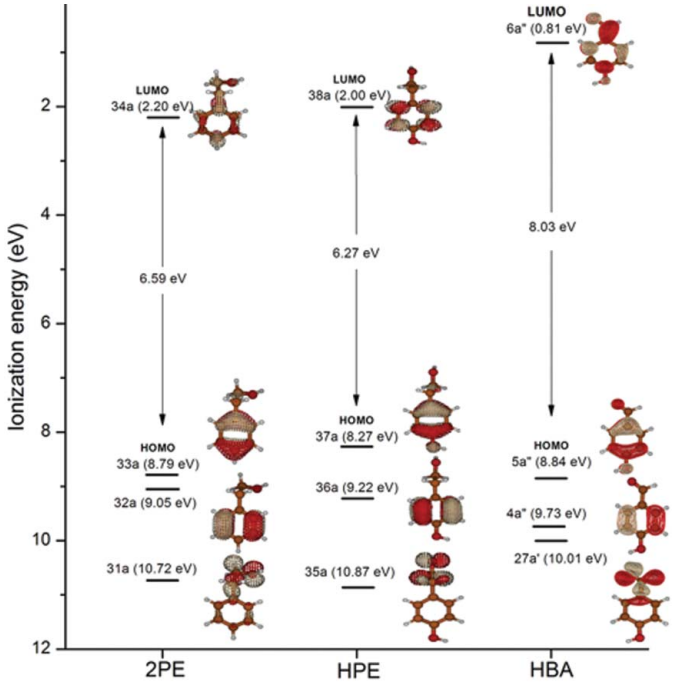

Figure 5
Energy diagram of frontier-occupied and virtual orbitals of 2PE, HPE and HBA. The energies are calculated using the OVGF/cc-pVTZ model and the charge densities of the orbitals are generated using the HF/cc-pVTZ level of theory.

4. Conclusions

The side-chain effects on the valence electronic structures of three biologically active compounds, 2PE, HPE and HBA, have been studied using combined experimental and theoretical X-ray photoelectron spectroscopy and IR spectroscopy. *Para*-hydroxyl substitution in HPE does not significantly alter the geometric properties of the aromatic ring with respect to 2PE. However, HBA, where the hydroxyethyl group of HPE is replaced by an aldehyde group, exhibits very small geometric differences from 2PE and HPE, which are associated with changes in their charge distributions. Similarities in the structures of the three biomolecules are reflected in the IR spectra, whereas the effects of solvent environments (such as water) split the IR spectral peak of OH by as much as 94 cm^{-1} in HPE. The vertical valence ionization spectra of 2PE, HPE and HBA were measured using X-ray photoemission spectroscopy, and have been assigned using the OVGF model. It is also found that, although the binding energies in the outermost valence region are very different among the three compounds, they exhibit similar orbital patterns; that is, the HOMOs and HOMO-1s are dominated by the phenyl ring, whereas the HOMO-2s are concentrated on the side chains.

One of the authors (APWA) acknowledges a Swinburne University Centenary Postgraduate Research Award. We acknowledge Sincrotrone Trieste for the beam time for proposal 20100265, and thank the staff of Elettra for providing good quality synchrotron light. The Australian Synchrotron is acknowledged for International Synchrotron Access Program travel grants. The National Computational Infrastructure (NCI) at the Australian National University (ANU) under the Merit Allocation Scheme (MAS), VPAC and Swinburne University Supercomputing Facilities are also acknowledged.

References

Ahn, E.-Y., Jiang, Y., Zhang, Y., Son, E. M., You, S., Kang, S.-W., Park, J.-S., Jung, J. H., Lee, B.-J. & Kim, D.-K. (2008). *Oncol. Rep.* **19**, 527–534.
Ayers, P. (2006). *Theor. Chem. Acc.* **115**, 370–378.
Bakke, J. M. & Chadwick, D. J. (1988). *Acta Chem. Scand. B*, **42**, 223–230.
Berrah, G. & Konetzka, W. A. (1962). *J. Bacteriol.* **83**, 738–744.
Bowman, J. P. (2007). *Mar. Drugs*, **5**, 220–241.
Cederbaum, L. S. (1975). *J. Phys. B*, **8**, 290–303.
Cederbaum, L. S. & Domcke, W. (1977). *Adv. Chem. Phys.* **36**, 205–344.
Chen, Y.-P. P., Ivanova, E., Wang, F. & Carloni, P. (2010). *Bioinformatics and its Applications*, in *Comprehensive Natural Products II: Chemistry and Biology*, Vol. 9, edited by L. N. Mander & H.-W. Liu, p. 569. Oxford: Elsevier.
Chervenkov, S., Karaminkov, R., Braun, J. E. & Neusser, H. J. (2006). *J. Chem. Phys.* **124**, 234302.
Chong, D. P., van Lenthe, E., van Gisbergen, S. & Baerends, E. J. (2004). *J. Comput. Chem.* **25**, 1030–1036.
Cossi, M., Barone, V., Cammi, R. & Tomasi, J. (1996). *Chem. Phys. Lett.* **255**, 327–335.
Cui, S., Hu, X., Chen, X. & Hu, Z. (2003). *Anal. Bioanal. Chem.* **377**, 370–374.
Cyrański, M. K. (2005). *Chem. Rev.* **105**, 3773–3811.
Dharmalingam, K., Ramachandran, K. & Sivagurunathan, P. (2006). *J Zhejiang Univ. Sci. A*, **7**, 1928–1931.
Dickinson, J. A., Hockridge, M. R., Kroemer, R. T., Robertson, E. G., Simons, J. P., McCombie, J. & Walker, M. (1998). *J. Am. Chem. Soc.* **120**, 2622–2632.
Dickinson, J. A., Joireman, P. W., Kroemer, R. T., Robertson, E. G. & Simons, J. P. (1997). *J. Chem. Soc. Faraday Trans.* **93**, 1467–1472.
Ehrhardt, S. M. (1984). Thesis. The Institute of Paper Chemistry, Lawrence University, Wisconsin, USA.
Fang, H. L. & Swofford, R. L. (1984). *Chem. Phys. Lett.* **105**, 5–11.
Frisch, M. J. *et al.* (2004). *Gaussian03.* Gaussian Inc., Wallingford, CT, USA.
Fronza, G., Fuganti, C., Grasselli, P., Servi, S., Zucchi, G., Barbeni, M. & Cisero, M. (2009). *J. Agric. Food Chem.* **43**, 439–443.
Ganesan, A., Wang, F. & Falzon, C. (2011). *J. Comput. Chem.* **32**, 525–535.
Godfrey, P. D., Jorissen, R. N. & Brown, R. D. (1999). *J. Phys. Chem. A*, **103**, 7621–7626.
Guchhait, N., Ebata, T. & Mikami, N. (1999). *J. Am. Chem. Soc.* **121**, 5705–5711.
Guzman-Lopez, O., Trigos, A., Fernandes, F. J., Yanez-Morales, M. J. & Saucedo-Castaneda, G. (2007). *World J. Microbiol. Biotechnol.* **23**, 1473–1477.
Ha, J. H., Lee, J. T., Kim, J. S., Yong, C. S., Kim, J. A., Ha, J. S. & Huh, K. J. (2000). *Ethnopharmacology*, **73**, 329–333.
Hirshfeld, F. L. (1977). *Theor. Chim. Acta*, **44**, 129–138.
Hockridge, M. R., Knight, M. S., Robertson, E. G., Simons, J. P., McCombie, J. & Walker, M. (1998). *Phys. Chem. Chem. Phys.* **1**, 407–413.
Huang, Z., Yu, W. & Lin, Z. (2006). *J. Mol. Struct. Theochem.* **758**, 195–202.
Iwasaki, F. (1977). *Acta Cryst.* B**33**, 1646–1648.
Jacobson, M., Adler, V. E., Kishaba, A. N. & Priesner, E. (2005). *Cell. Mol. Life Sci.* **32**, 964–966.
Jalkanen, K. J., Degtyarenko, I. M., Nieminen, R. M., Cao, X., Nafie, L. A., Zhu, F. & Barron, L. D. (2008). *Theor. Chem. Acc.* **119**, 191–210.
Jasinski, J. P., Butcher, R. J., Narayana, B., Swamy, M. T. & Yathirajan, H. S. (2008). *Acta Cryst.* E**64**, o187.
Jirovetz, L., Buchbauer, G., Schmidt, E., Denkova, Z., Slavchev, A., Stoyanova, A. & Geissler, M. (2008). *J. Essent. Oil Res.* **20**, 82–85.
Karaminkov, R., Chervenkov, S. & Neusser, H. J. (2008). *J. Phys. Chem. A*, **112**, 839–848.
Kim, H. J., Hwang, I. K. & Won, M. H. (2007). *Brain Res.* **1181**, 130–141.
Leeuwen, R. van & Baerends, E. J. (1994). *Phys. Rev. A*, **49**, 2421–2431.
Li, M. (2006). PhD thesis. Hong Kong University of Science and Technology, Hong Kong.
Liu, J. & Mori, A. (1993). *Neuropharmacology*, **32**, 659–669.
Mardis, K. L., Brune, B. J., Vishwanath, P., Giorgis, B., Payne, G. F. & Gilson, M. K. (2000). *J. Phys. Chem. B*, **104**, 4735–4744.
Mart, H., Yürüka, H., Şaçak, M., Muradoğlu, V. & Vilayetoğlu, A. R. (2004). *Polym. Degrad. Stab.* **83**, 395–398.
Mons, M., Robertson, E. G. & Simons, J. P. (2000). *J. Phys. Chem. A*, **104**, 1430–1437.
Mons, M., Robertson, E. G., Snoek, L. C. & Simons, J. P. (1999). *Chem. Phys. Lett.* **310**, 423–432.
Müller, W. E. G., Falke, D., Heicke, B. & Zahn, R. K. (2005). *Arch. Virol.* **40**, 205–214.
Niessen, W. von, Schirmer, J. & Cederbaum, L. S. (1984). *Comput. Phys. Rep.* **1**, 57–125.
NIST (2009). *NIST Chemistry WebBook*, NIST Standard Reference Database Number 69, edited by P. J. Linstrom and W. G. Mallard. National Institute of Standards and Technology, Gaithersburg, MD 20899, USA. [http://webbook.nist.gov/ (retrieved 28 October 2011).]
Panja, S. S. & Chakraborty, T. (2003). *J. Phys. Chem. A*, **107**, 10984–10987.

Patey, M. D. & Dessent, E. H. (2002). *J. Phys. Chem A*, **106**, 4623–4631.
Plekan, O., Feyer, V., Richter, R., Coreno, M., de Simone, M., Prince, K. C. & Carravetta, V. (2007*a*). *Chem. Phys. Lett.* **442**, 429–433.
Plekan, O., Feyer, V., Richter, R., Coreno, M., de Simone, M., Prince, K. C. & Carravetta, V. (2007*b*). *J. Electron Spectrosc. Relat. Phenom.* **155**, 47–53.
Plekan, O., Feyer, V., Richter, R., Coreno, M., de Simone, M., Prince, K. C. & Carravetta, V. (2007*c*). *J. Phys. Chem. A*, **111**, 10998–11005.
Pouchert, C. J. (1985). Editor. *The Aldrich Library of FT-IR Spectra*, Vol. 1, ed. I, p. 1166D.
Robertson, E. G. & Simons, J. P. (2000). *Phys. Chem. Chem. Phys.* **3**, 1–18.
Sajan, D., Erdogdu, Y., Kuruvilla, T., Joe, I. H. (2010). *J. Mol. Struct.* **983**, 12–21.
Sakai, M., Hirata, H., Sayama, H., Sekiguchi, K., Itano, H., Asai, T., Dohra, H., Hara, M. & Watanabe, N. (2007). *Biosci. Biotechnol. Biochem.* **71**, 2408–2419.
Schmidt, M. W., Baldridge, K. K., Boatz, J. A., Elbert, S. T., Gordon, M. S., Jensen, J. H., Koseki, S., Matsunaga, N., Nguyen, K. A., Su, S. J., Windus, T. L., Dupuis, M. & Montgomery, J. A. (1993). *J. Comput. Chem.* **14**, 1347–1363.
Scott, A. P. & Radom, L. (1996). *J. Phys. Chem.* **100**, 16502–16513.
Selvam, L., Chen, F. & Wang, F. (2010). *Chem. Phys. Lett.* **500**, 327–333.
Stenuit, G., Castellarin-Cudia, C., Plekan, O., Feyer, V., Prince, K. C., Goldoni, A. & Umari, P. (2010). *Phys. Chem. Chem. Phys.* **12**, 10812–10817.
Tieman, D. M., Loucus, H. M., Kim, J. Y., Clark, D. G. & Klee, H. J. (2007). *Phytochemistry*, **68**, 2660–2669.
Wang, F., Downton, M. & Kidwani, N. (2005). *J. Theor. Comput. Chem.* **4**, 247–264.
Wang, F., Zhu, Q. & Ivanova, E. P. (2008). *J. Synchrotron Rad.* **15**, 624–631.
Wiberg, K. B., Hammer, J. D., Keith, T. A. & Zilm, K. (1999). *J. Phys. Chem.* **103**, 21–27.
Wickrama Arachchilage, A. P., Wang, Y. & Wang, F. A. (2011). *Theor. Chem. Acc.* **130**, 965–979.
Wiseman, S. A., Tijburg, L. B. & van de Put, F. H. (2002). *Lipids*, **37**, 1053–1057.
Zakrzewski, V. G. & Ortiz, J. V. (1995). *Intl. J. Quantum Chem.* **53**, 583–590.
Zakrzewski, V. G. & von Niessen, W. (1993). *J. Comput. Chem.* **14**, 13–18.